

Time delay in valence shell photoionization of noble gas atoms

A. S. Kheifets*

Research School of Physical Sciences, The Australian National University, Canberra ACT 0200, Australia

(Dated: December 18, 2012)

We use the non-relativistic random phase approximation with exchange to perform calculations of valence shell photoionization of Ne, Ar, Kr and Xe from their respective thresholds to photon energy of 200 eV. The energy derivative of the complex phase of the photoionization matrix elements is converted to the photoelectron group delay that can be measured in attosecond streaking or two-photon transitions interference experiments. Comparison with reported time delay measurements in Ne and Ar at a few selected photon energies is made. Systematic mapping of time delay across a wide range of photon energies in several atomic targets allows to highlight important aspects of fundamental atomic physics that can be probed by attosecond time delay measurements.

PACS numbers: 32.30.Rj, 32.70.-n, 32.80.Fb, 31.15.ve

I. INTRODUCTION

Time delay in atomic photoionization has become an active and rapidly expanding field of research after pioneering experiments on attosecond streaking [1] and reconstruction of attosecond bursts by interference of two-photon transitions [2]. Both techniques use the XUV pump and IR probe pulses to ionize the target atom and to obtain timing information on the photoemission process. In attosecond streaking, the varying time delay between the the pump and probe pulses is mapped onto the photoelectron kinetic energy. The whole valence band is projected onto a photoelectron kinetic energy map (the so-called spectrogram) which is then modeled, in the strong field or Coulomb-Volkov approximations, with the photoionization time delay being treated as a fitting parameter. This measurement revealed a relative time delay of 21 ± 5 as between photoemission from the $2p$ and $2s$ shells in Ne at 106 eV photon energy. The positive sign of the relative time delay indicates that emission of the photoelectron from the $2p$ shell is seemingly delayed relative to that from the $2s$ shell. This result was interpreted in terms of the Wigner time delay (or photoelectron group delay, both terms will be used interchangeably in the present contents) which is defined as the energy derivative of the complex phase of the photoionization matrix element [1, 3]. More details on the Wigner time delay theory can be found in the review article by de Carvalho and Nussenzveig [4].

In the two-photon interferometric technique, the varying time delay between the pump and probe pulses is mapped onto the two-photon sidebands (SB) which exhibit an oscillating pattern of peaks and troughs. The phase of these oscillations depends on the sum of time delays in the XUV photon absorption (atomic photoionization) and subsequent IR photon absorption (continuum-continuum transition). The latter is modeled using the lowest order perturbation theory and asymptotic forms

of the continuum wave functions thus allowing to obtain the former from an experimental measurement [5]. By reconstructing the oscillations of the SB 22 to 26 of the titanium:sapphire laser at 800 nm, Klünder *et al* [2] reported the relative time delay between the photoelectron emission from the $3s$ and $3p$ shells of Ar in the photon energy range of 34 to 40 eV. Whether the $3p$ electron was delayed relative to the $3s$ one or vice versa was found to depend on the photon energy. This measurement was repeated later by Guénot *et al.* [6] and the sign of the relative time delay was reversed with the $3s$ photoelectron being delayed relative to the $3p$ one near the top end of the photon energy scale.

This repeated measurement was prompted by observation that the photon energy of 40 eV fell very close to the Cooper's minimum of the $3s$ shell. Photoionization process in this region is driven very strongly by the many-electron correlation between the $3s$ and $3p$ shells [7]. Such a process cannot be theoretically described using an independent electron model like the Hartree-Fock (HF) theory. So the interpretation of the two-photon interferometric measurement Klünder *et al* [2] based on this theory should be re-evaluated. A more adequate model that accounts for inter-shell correlation in noble gas atoms is the random phase approximation with exchange (RPAE or, shorter, RPA, both acronyms are used here interchangeably) [8]. However, even after including the RPA corrections, the agreement between theory and experiment did not improve [6].

Theoretical interpretation of the attosecond streaking measurement of Schultze *et al* [1] is also not straightforward. The group delay difference between the $2p$ and $2s$ shells in Ne calculated in the HF approximation is only 6.2 as [3]. With the added RPA correction of 2.2 as, it accounts for less than a half of the experimental value of 21 ± 5 as. A more accurate modeling that accounted both the XUV and IR fields returned a similar value of 10.2 ± 1.3 as [9]. This prompted several authors to question the accuracy of attosecond streaking measurements [10, 11, 12]. This question is still being debated.

For the purpose of the present paper, we presume that the time delay in the Wigner's sense, i.e. the photoelec-

*Electronic address: A.Kheifets@anu.edu.au

tron group delay, can be measured experimentally. To support such measurements and to provide them with a “road map” of consistent theoretical data, we embark on the systematic studies of the time delay in a series of noble gas atoms from Ne to Xe across a wide range of photon energies. We demonstrate that such a systematic study allows to highlight important aspects of fundamental atomic physics that can be revealed by attosecond time delay measurements.

The paper is organized as follows. In Sec. II we introduce our computational models for the independent electron descriptions and that with account for the inter-shell correlations. In Sec. III we present our numerical results for outer valence ns and np shells in Ne and Ar and ns , np , $(n-1)d$ shells in Kr and Xe. We conclude in Sec. IV by revealing the systematic trends in time delay of noble gases driven by the peculiarities of the elastic scattering phases and many-electron correlations.

II. THEORETICAL MODEL

1. Independent electron HF model

We adopt the photoionization formalism as outlined in the monograph [13]. We evaluate the one-photon dipole matrix element $\langle \psi_{\mathbf{k}}^{(-)} | \hat{z} | \phi_i \rangle$ of the transition from a bound state i to an incoming continuous wave with the given photoelectron momentum \mathbf{k} . The magnitude of the momentum is restricted by the energy conservation $E \equiv k^2/2 = \omega + \varepsilon_i$, where ω is the photon energy. The atomic units are used throughout the paper with $e = m = \hbar = 1$ and the atomic unit of time equal to 24 as. We split the radial and angular dependence in the initial state $\phi_i(\mathbf{r}) = Y_{l_i m_i}(\hat{\mathbf{r}}) R_{n_i l_i}(r)$ and use the partial wave expansion in the final state

$$\psi_{\mathbf{k}}^{(-)}(\mathbf{r}) \propto \sum_{lm} i^l e^{-i\delta_l(E)} Y_{lm}^*(\hat{\mathbf{k}}) Y_{lm}(\hat{\mathbf{r}}) R_{kl}(r), \quad (1)$$

where the proportionality constant depends on the continuum normalization. We align the quantization axis z with the polarization axis of light and write the dipole operator in the length gauge as $\hat{z} = \sqrt{4\pi/3} r Y_{10}(\hat{\mathbf{r}})$. We perform the spherical integration to arrive to the following expression:

$$\langle \psi_{\mathbf{k}} | \hat{z} | \phi_i \rangle \propto \sum_{\substack{l=l_i \pm 1 \\ m=m_i}} e^{i\delta_l(E)} i^{-l} Y_{lm}(\hat{\mathbf{k}}) \times \begin{pmatrix} l & 1 & l_i \\ m & 0 & m_i \end{pmatrix} \langle kl || d || n_i l_i \rangle \quad (2)$$

Here the reduced dipole matrix element, stripped of all the angular momentum projections, is defined as

$$\langle kl || d || n_i l_i \rangle = \hat{l}_i \begin{pmatrix} l & 1 & l_i \\ 0 & 0 & 0 \end{pmatrix} \int r^2 dr R_{kl}(r) r R_{n_i l_i}(r), \quad (3)$$

where $\hat{l} = \sqrt{2l+1}$. The partial photoionization cross section for the transition from an occupied state $n_i l_i$ to the photoelectron continuum state kl is calculated as

$$\sigma_{n_i l_i \rightarrow kl} = \frac{4}{3} \pi^2 \alpha a_0^2 \omega |\langle kl || d || n_i l_i \rangle|^2. \quad (4)$$

Here α the fine structure constant and a_0 the Bohr radius.

The basis of occupied atomic states $|n_i l_i\rangle$ is defined by the self-consistent HF method and calculated using the computer code [14]. The continuum electron states $\langle kl|$ are defined within the frozen-core HF approximation and evaluated using the computer code [15]. These states are found in the combined field of the nucleus and the HF potential of the frozen electron core. So the photoelectron scattering phase $\delta_l(E)$ delivered by this method contains both the long-range Coulomb and the short-range Hartree-Fock components.

We note that the reduced matrix element (3) is real and thus the complex phase of the dipole matrix element (2) is defined by the scattering phases $\delta_{l_i \pm 1}(E)$. According to the Fano’s propensity rule [16], the dipole transition with the increased momentum $l = l_i + 1$ is usually dominant and thus the photoemission time delay is simply $\tau_l = d\delta_l/dE$.

2. Inter-shell correlation

To include inter-shell correlation effects, we employ the RPA model [13]. In this approximation, the reduced dipole matrix element (3) is replaced by its correlated counterpart $\langle kl || D || n_i l_i \rangle$ which accounts for correlation between different atomic shells. This correlated matrix element is found as a solution of the system of the integral equations:

$$\langle kl || D || n_i l_i \rangle = \langle kl || d || n_i l_i \rangle + \frac{1}{3} \lim_{\varepsilon \rightarrow 0^+} \sum_{\substack{p'l' \\ n_j l_j}} \left[\frac{\langle p'l' || D || n_j l_j \rangle \langle n_j l_j k l || V || p'l' n_i l_i \rangle}{\omega - p'^2/2 + \varepsilon_j + i\varepsilon} + \frac{\langle n_j l_j || D || p'l' \rangle \langle p'l' k l || V || n_j l_j n_i l_i \rangle}{\omega + p'^2/2 - \varepsilon_j} \right], \quad (5)$$

These equations are represented graphically in Fig. 1. Here the straight line with an arrow to the left or right represents electron (continuum) or hole (bound) states, respectively. The wavy line exhibits the Coulomb interaction, which contains both the direct and the exchange parts. That explains the term exchange in the name RPA(E). The dashed line is used to display a photon of the frequency ω . The shaded circle is used to represent the correlated dipole matrix element whereas the bare matrix element is exhibited by a three-pronged vertex. The Coulomb interaction matrices $\langle n_j l_j k l || V || p'l' n_i l_i \rangle$ and $\langle p'l' k l || V || n_i l_i n_j l_j \rangle$, describe the so-called time-forward and time-reverse correlation processes which are exhibited by the second and third diagrams (from left to right).

We solve the system of integral equations (5) using a slightly modified version of the computer code [17]. The energy integration in the time-forward term of Eq. (5) (second line) contains a pole and the RPA matrix element acquires an imaginary part and therefore an extra phase $\arg\langle kl||D||n_i l_i\rangle$. However, this phase does not enter the partial photoionization cross section $n_i l_i \rightarrow kl$ which is obtained from the squared matrix element (5):

$$\sigma_{n_i l_i \rightarrow kl} = \frac{4}{3} \pi^2 \alpha a_0^2 \omega |\langle kl||D||n_i l_i\rangle|^2. \quad (6)$$

To get access to the phase information, one has to evaluate the angular asymmetry parameter defined as

$$\beta_{n_i l_i \rightarrow kl} = \left[(2l+1)(|D_{l+1}|^2 + |D_{l-1}|^2) \right]^{-1} \quad (7)$$

$$\times \left\{ (l+2)|D_{l+1}|^2 + (l-1)|D_{l-1}|^2 + 6\sqrt{l(l+1)} \operatorname{Re} \left(D_{l+1} D_{l-1}^* e^{i(\delta_{l+1} - \delta_{l-1})} \right) \right\}$$

Here we used a shortcut D_l for the RPA matrix element (5). The angular asymmetry parameter β contains the phase difference between the two photoionization channels $l = l_i \pm 1$ when $l_i \neq 0$. The photoelectron group delay, which is the energy derivative of the phase of the complex photoionization matrix element, gives an alternative access to the phase information. It is evaluated as the imaginary part of the logarithmic derivative

$$\tau = \operatorname{Im} \left[f'(E)/f(E) \right] \quad (8)$$

where

$$f(E) \propto \sum_{\substack{l=l_i \pm 1 \\ m=m_i}} e^{i\delta_l(E)} i^{-l} Y_{lm}(\hat{\mathbf{k}}) \quad (9)$$

$$\times \begin{pmatrix} l & 1 & l_i \\ m & 0 & m_i \end{pmatrix} \langle kl||D||n_i l_i\rangle$$

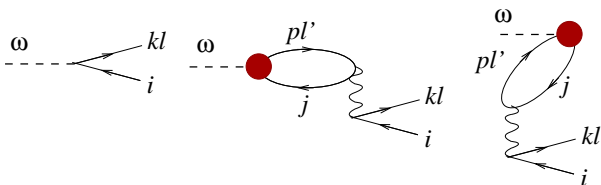


FIG. 1: Graphical representation of the RPA equations (5). Left: non-correlated dipole matrix element. Center: time-forward process. Right: Time-reverse process.

III. NUMERICAL RESULTS

A. Neon 2s and 2p shells

On the top panel of Fig. 2 we present the partial photoionization cross-sections of valence shell photoionization of Ne. The HF cross-sections (4) are shown by

the dashed (blue) lines and the RPA cross-sections (6) are exhibited by the solid (red) line. The recommended experimental data by Bizau and Wulleumier [18] are displayed with error bars. In the RPA calculation, we substitute the HF bound state energies with the experimental ionization thresholds $\epsilon_{2p_{3/2}} = 21.56$ eV and $\epsilon_{2s} = 48.47$ eV [19] which are indicated on the upper boundary of the panel. We see that account for the RPA correlation between the 2s and 2p shells improves the calculated cross-sections and makes them closer to the experimental data.

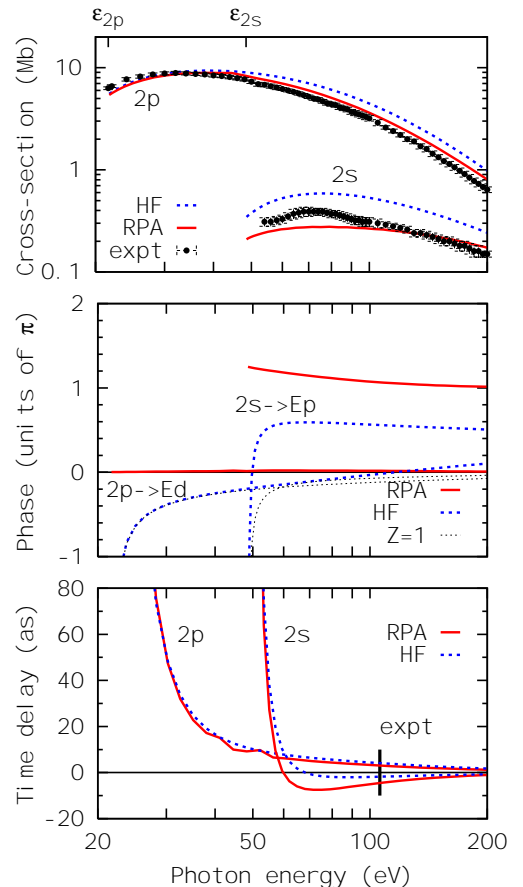


FIG. 2: (Color online) Top: the partial photoionization cross-sections of the 2s and 2p shells of Ne. The HF and RPA calculations are shown by the dashed (blue) and solid (red) lines, respectively. The recommended experimental data by Bizau and Wulleumier [18] are displayed with error bars. Middle: elastic scattering phases in the field of the Ne^+ ion for the $2s \rightarrow Ep$ and the dominant $2p \rightarrow Ed$ channels (dotted blue line) and the RPA phases (solid red line). The thin dotted line visualizes the Coulomb phase with $Z = 1$. Bottom: the phase derivatives are converted to the units of the group delay. The vertical bar at the photon energy of 106 eV visualizes the relative time delay between the 2p and 2s shells of 21 as as measured by Schultze *et al* [1]

On the middle panel, we show the elastic scattering phases in the field of the Ne^+ ion for the $2s \rightarrow Ep$ and the

dominant $2p \rightarrow Ed$ channels. The HF phases $\delta_p(E)$ and $\delta_d(E)$ are plotted with the dashed (blue) line. The RPA phases $\arg\langle kp||D||2s\rangle$ and $\arg\langle kd||D||2p\rangle$ are displayed with the solid (red) line. The thin dotted line visualizes the Coulomb phase $\sigma_l(E) = \arg\Gamma\left(1+l-iZ_{\text{eff}}/\sqrt{2E}\right)$ with the effective charge $Z_{\text{eff}} = 1$. This phase shows the contribution of the long-range Coulomb potential to the HF phase $\delta_l(E)$ which is strongly dominant at small kinetic energies of the photoelectron. The phase shift due to the short range potential, i.e. the difference of the total phase and the Coulomb phase, is related to the quantum defect according to the Levinson-Seaton theorem $\delta_l(k \rightarrow 0) - \sigma_l(k \rightarrow 0) = \mu_l(\infty)\pi$ [20]. For a neutral target, the scattering phase at zero energy is related to the number of the occupied target states N_l by the Levinson's theorem $\delta_l(k \rightarrow 0) = N_l\pi$. We see a clear cross-over between the Coulomb behavior of the HF phase towards the Levinson behavior. Indeed, in the absence of the Coulomb contribution, the $2s \rightarrow Ep$ phase would tend to one unit of π as there is one occupied $2p$ shell in the Ne^+ ion. Similarly, the the $2p \rightarrow Ed$ phase would tend to zero as there are no occupied d -shells left behind.

The RPA phase in the $2p \rightarrow Ed$ channel is hardly distinguishable from zero. This observation is consistent with a very small change that the RPA correction causes to the partial photoionization cross-section shown on the top panel. The RPA phase in the $2s \rightarrow Ep$ channel is large but rather flat and changes slowly with the photon energy. This is consistent with the $2s$ partial photoionization cross-section which is affected by the inter-shell correlation with $2p$ across the whole range of the studied photon energies.

The bottom panel of Fig. 2 displays the photoelectron group delay calculated as the energy derivative of the phase of the photoionization matrix element. The HF time delay in the dominant photoionization channel is calculated as $\tau_l^{\text{HF}}(\text{as}) = k^{-1}d\delta_l/dk \times 24$. Here $E = k^2/2$ is the photoelectron energy in atomic units and one unit of time is equal to 24 attoseconds. In the existing code, the continuous electron orbitals are calculated on the regular momentum grid and numerical differentiation over the momentum, rather than energy, is easier to implement. The fine grid of 0.05 au of photoelectron momentum is sufficient for an accurate numerical differentiation. Similarly, the RPA time delay is calculated as $\tau^{\text{RPA}}(\text{as}) = \text{Im}\left[k^{-1}f'(k)/f(k)\right] \times 24$. Here the photoionization amplitude (9) is evaluated in the z -axis direction. In this case $Y_{lm}(\hat{\mathbf{k}}||\hat{\mathbf{z}}) \propto \delta_{m0}$ and no summation over the angular momentum projection in the initial state is needed. We see that the HF time delay in the dominant $2p \rightarrow Ed$ channel accounts for almost the whole time delay in photoemission from the $2p$ shell. There is some oscillation visible due to the autoionizing resonances near the $2s$ threshold which is absent in the HF approximation. Overall, the $2p$ time delay is always positive and rapidly decreasing function of the photon energy. This is explained by the monotonously decreasing HF phase

in the d -partial wave which is driven by the Coulomb logarithmic singularity. The situation is different in the $2s \rightarrow Ep$ channel. Here the HF phase crosses over from the Coulomb behavior at low photoelectron kinetic energy to the Levinson behavior at larger energies. In result, the phase derivative and, consequently, the time delay change their sign from positive and negative towards the larger photon energies. The RPA correction to the time delay is always negative. Hence the photoemission from the $2s$ shell seems to be ahead of that of the $2p$ shell at around 100 eV photon energy mark where the measurement of Schultze *et al* [1] was taken (shown as a vertical bar in the figure). However, the combined HF and RPA result of 8.4 as is less than a half of the reported experimental value of 21 ± 5 as.

1. Argon 3s and 3p shells

An analogous set of data for Ar $3s$ and $3p$ shells is shown in Fig. 3. On the top panel we make a comparison of the HF (dashed blue line) and the RPA (solid red line) partial photoionization cross-sections with the experimental data by Möbus *et al* [21] for $3s$ shell and by Samson and Stolte [22] for the sum of $3s$ and $3p$ shells. The experimental ionization thresholds $\epsilon_{3p_{3/2}} = 15.76$ eV and $\epsilon_{3s} = 29.24$ eV [19] are indicated on the upper boundary of the panel. These partial photoionization cross-sections are qualitatively different from those of Ne shown in Fig. 2. Firstly, the $3p$ cross-section in Ar displays the Cooper's minimum whereas the nodeless $2p$ orbital does not [23]. Second, the inter-shell correlation changes completely the $3s$ cross-section which also display a deep Cooper-like minimum at a slightly smaller photon energy. The RPA calculation reproduce these features in good agreement with the experiment.

The HF phases in Ar behave similarly to the analogous case of Ne except that the $3s \rightarrow Ep$ phase would tend to 2π in the absence of the Coulomb singularity as there are two occupied p -shells in the Ar^+ ion. The RPA phases in Ar are very different from Ne. When the cross-section goes through the Cooper's minimum, the corresponding phase makes a jump of π in the $3s \rightarrow Ep$ amplitude, and $-\pi$ in the $3p \rightarrow Ed$ amplitude. This jump is easy to understand. If the amplitude was real and had a node, it would simply change its sign which would amount to adding a phase factor of π in the complex number representation.

This jump of π has a dramatic effect on the time delay which is shown on the bottom panel of Fig. 3. It drives the time delay in the $3s$ shell to very larger numbers in several hundreds of attoseconds. The situation is less dramatic for the $3p$ shell. Here the normally weak transition $3p \rightarrow Es$ takes over near the Cooper's minimum of the strong $3p \rightarrow Ed$ transition and the resulting time delay does not go below -100 as. We note that there is a strong variation of phase near the autoionization resonances in the $3p$ photoionization which is seen on the

SB	22	24	26
ω (eV)	34.1	37.2	40.3
$\tau_{3s} - \tau_{3p}$ (as)			
HF	3	-36	-38
RPA	76	53	215
Expt	70	-30	50

TABLE I: Relative time delay between the photoemission from the $3s$ and $3p$ shells $\tau_{3s} - \tau_{3p}$ in Ar at three fixed photon energies corresponding to the SB 22 to 26 in the experiment of Guénot et al. [6]. The experimental uncertainty is ± 50 as.

top panel of Fig. 3. We do not show this variation in the phase and time delay plots for clarity of presentation. Anyway, these resonances are far too narrow to be detected in time delay measurements at present energy resolution.

On the upper boundary of the bottom panel, we indicate the photon energies corresponding to the SB 22 to 26 of the titanium:sapphire laser at 800 nm used in the two-photon interferometric experiments [2, 6]. We see that at this photon energy range, the RPA correction changes completely the sign of the relative $3p/3s$ time delay. In the HF approximation, the $3p$ photoemission is delayed more than the $3s$ ones. The inter-shell correlation changes this ordering completely. With the RPA correction, it is the $3s$ that is delayed more than the $3p$. This is an important, strong and qualitative result which is related to the Cooper's minima in the corresponding partial photoionization cross-sections.

This strong modification of the relative time delay between the $3p$ and $3s$ shells in Ar is more clearly seen in Table I where we present the time delay difference $\tau_{3s} - \tau_{3p}$ in the HF and RPA approximations and compare it with the experimental data of Guénot et al. [6]. Even a fairly large uncertainty of ± 50 as cannot reconcile the experimental data with neither of the calculations.

2. Krypton $4p$, $4s$ and $3d$ shells

Our results for the $4p$, $4s$ and $3d$ photoionization of Kr are displayed in Fig. 4. On the top panel we make a comparison of the HF (dashed blue line) and the RPA (solid red line) partial photoionization cross-sections with the experimental data of Ehresmann et al. [24] for $4s$ and of Samson and Stolte [22] for $4p + 3d$ (error bars). The data from Aksela et al. [25] for $3d$ are displayed with asterisks. The experimental ionization thresholds $\epsilon_{4p_{3/2}} = 14.00$ eV, $\epsilon_{4s} = 27.51$ eV [19] and $\epsilon_{3d_{5/2}} = 93.83$ eV [26] are indicated on the upper boundary of the panel. The $4p$ and $4s$ cross-sections in Kr behave similarly to the $3p$ and $3s$ cross-sections in Ar (see the top panel of Fig. 3). The $4p \rightarrow Ed$ cross-section goes through its Cooper's minimum which is offset somewhat by the weaker $4p \rightarrow Es$ channel. So the total $4p$

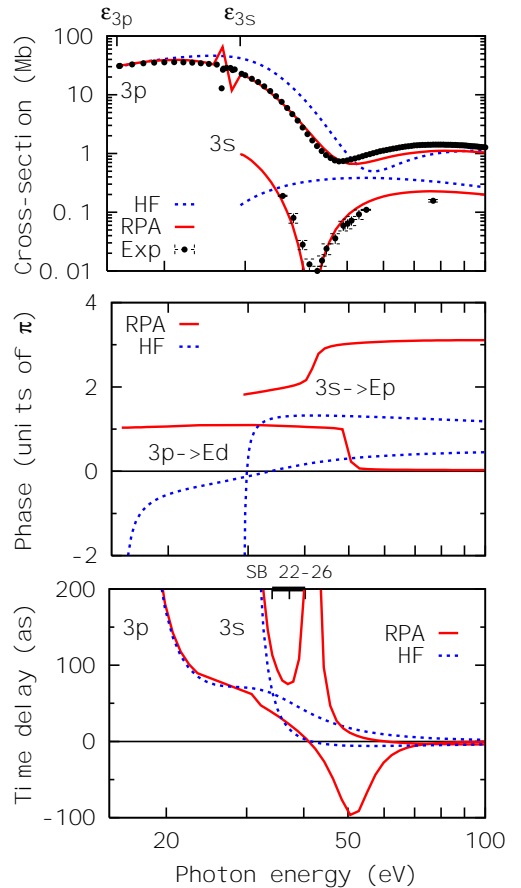


FIG. 3: (Color online) Top: the partial photoionization cross-sections of the $3s$ and $3p$ shells of Ar. The HF and RPA calculations are shown by the dashed (blue) and solid (red) lines, respectively. The experimental data by Möbus *et al* [21] for $3s$ and by Samson and Stolte [22] for $3s + 3p$ are displayed with error bars. Middle: elastic scattering phases in the field of the Ar^+ ion for the $3s \rightarrow Ep$ and the dominant $3p \rightarrow Ed$ channels (dotted blue line) and the RPA phases (solid red line). Bottom: the phase derivatives are converted to the units of the group delay.

cross-section displays a shoulder rather than a true minimum. The $4s$ cross-section is driven strongly by its inter-shell correlation with $4p$ to a very deep minimum which is missed completely in the HF approximation. The $3d$ cross-section from its threshold displays a strong maximum associated with its shape resonance. This resonance is known to be due to electron correlation within a single shell [27] and indeed the $3d$ photoionization cross-section is well described by the HF approximation.

The HF phases in Kr (middle panel of Fig. 4) behave similarly to the analogous cases of Ne and Ar except that the $4s \rightarrow Ep$ phase would tend to 3π and the $4p \rightarrow Ed$ phase would tend to π in the absence of the Coulomb singularity. The RPA phases in Kr are also similar to Ar. Every time the cross-section goes through the Cooper's minimum, the corresponding phase makes a jump of π :

upwards in the $4s \rightarrow Ep$ amplitude and downwards in the $4p \rightarrow Ed$ amplitude. The RPA phase in the $3d \rightarrow Ef$ transition is rather stationary.

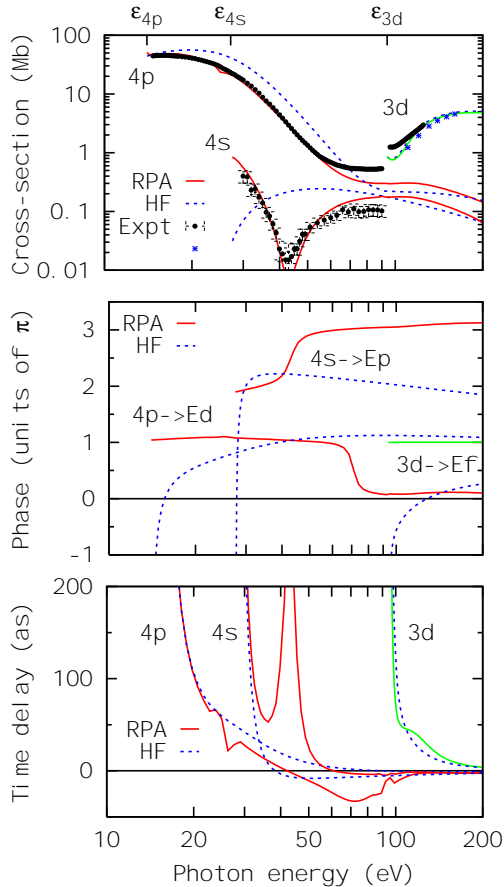


FIG. 4: (Color online) Top: the partial photoionization cross-sections of Kr. The HF and RPA calculations are shown by the dashed (blue) and solid (red for $4s$, $4p$ and green for $3d$) lines, respectively. The experimental data by Ehresmann et al. [24] for $4s$ and by Samson and Stolte [22] for $4p + 3d$ are displayed with error bars. The data from Aksela et al. [25] for $3d$ are displayed with asterisks. Middle: elastic scattering phases in the field of the Ar^+ ion for the $4s \rightarrow Ep$ and the dominant $4p \rightarrow Ed$ channels (dotted blue line) and the RPA phases (solid red line). Bottom: the phase derivatives are converted to the units of the group delay.

This behavior of the phases translates into the corresponding time delays plotted on the bottom panel of Fig. 4. The RPA time delay in $4p$ shell is not dramatically different from the HF calculation. Even though the dominant $4p \rightarrow Ed$ transition displays a Cooper’s minimum, it is offset by the weak $4p \rightarrow Es$ transition and is not as prominent in the total $4p$ cross-section as in the $3p$ cross-section of Ar. There are some variation of the time delay near the autoionizing resonances close to the $4s$ threshold which are seen in the RPA calculation but not in HF one. The time delay in the $3d$ shell is almost entirely due to intra-shell effects and the HF and RPA

results are very close. The situation is very different in the $4s$ shell where the time delay is strongly affected by the inter-shell correlation with the $4p$ shell and reaches 300 as in its peak. Similarly to Ar, there is a complete reversal of the relative time delay between the $4p$ and $4s$ shells in the RPA calculation in comparison with the HF one.

3. Xenon $5p$, $5s$ and $4d$ shells

The analogous set of data for the $5p$, $5s$ and $4d$ shells of Xe is presented in Fig. 5. On the top panel we compare the partial photoionization cross-sections in the HF (dashed blue line) and RPA (solid red line) approximations with the experimental data [28, 29] which are shown with the blue asterisks for $5s$ and error bars for $5p$ and $4d$. The experimental ionization thresholds $\epsilon_{5p_{3/2}} = 12.13$ eV, $\epsilon_{2s} = 23.40$ eV [19] and $\epsilon_{4d_{5/2}} = 67.50$ eV [30] are indicated on the upper boundary of the panel.

Below the $4d$ ionization threshold, the $5s$ and $5p$ cross-sections in Xe behave similarly to the $4s$ and $4p$ shells in Kr (top panel of Fig. 4). However, above this threshold, the $4d$ shell goes through a very steep shape resonance, sometimes even called a “giant resonance”. This resonance is then turns into a Cooper’s minimum. By strong inter-shell interaction, this behavior is replicated in the $5p$ and $5s$ partial photoionization cross-sections which are well reproduced by the RPA calculation. Accordingly, the corresponding RPA phases displays steep π jumps (middle panel) which are reflected in the corresponding time delays (bottom panel). In the case of the $5s$ shell, the RPA phase jump near the Cooper’s minimum merges with the Coulomb singularity and produces a very large, nearly 300 as time delay at the photon energies below 30 eV. The $5p$ shell shows a large and negative time delay due to its Cooper’s minimum at around 50 eV. Both the $5s$ and $5p$ shells display a large and negative time delay near the local cross-section minima around 150 eV induced by the correlation with the $4d$ shell. The time delay in the $4d$ shell is driven from the strongly positive due to the Coulomb singularity at low photon energies to a large negative jump near the Cooper’s minimum at about 180 eV. At larger energies, the cross-sections are rather structureless and there is no significant time delay variations.

A phase jump of π , smoothed by the interaction between the two channels, has already been observed both theoretically and experimentally by analyzing the anisotropy parameter in photoionization of Xe $5p$ shell [31]. According to Eq. (7), this parameter contains the phase shift between the two photoionization channels with $l = l_i \pm 1$. In the case of $5p$ photoionization, these are $5p \rightarrow Ed$ and $5p \rightarrow Es$ transitions. Their partial photoionization cross-sections and the relative phase shift are presented on the top and bottom panels of Fig. 6. On both panels, we show the present RPA and HF calculations displayed with the solid red and blue dotted lines,

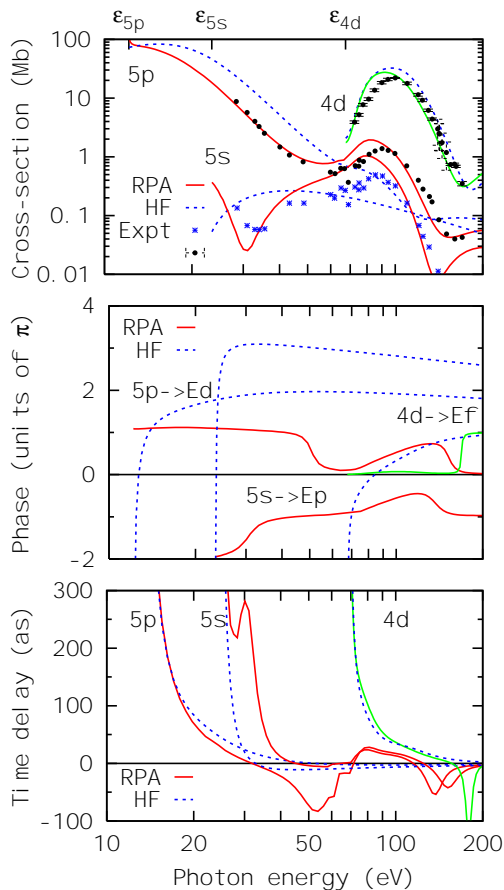


FIG. 5: (Color online) Top: the partial photoionization cross-sections of Xe. The HF and RPA calculations are shown by the dashed (blue) and solid (red for $5s$, $5p$ and green for $4d$) lines, respectively. The experimental data from Becker et al. [28] and Fahlman et al. [29] are shown with asterisks for $5s$ and error bars for $5p$ and $4d$. Middle: elastic scattering phases in the field of the Ar^+ ion for the $5s \rightarrow Ep$ and the dominant $5p \rightarrow Ed$ and $4d \rightarrow Ef$ channels (dotted blue line) and the RPA phases (solid red line). Bottom: the phase derivatives are converted to the units of the group delay.

respectively. On the bottom panel, we exhibit the RPA (open circles) and HF (filled circles) phase shifts reported by [31].

On the top panel of Fig. 6 we observe a significant shift of the Cooper's minimum in the $5p \rightarrow Ed$ channel towards the lower photon energies and appearance of the secondary minimum due to the correlation with the $4d$ shell. In the meantime, the inter-shell correlation does not change the $5p \rightarrow Es$ partial photoionization cross-section in such a dramatic way. Accordingly, on the bottom panel of Fig. 6, we see a strong variation of the RPA phase shift with the two successive π jumps near the Cooper's minima of the $5p \rightarrow Ed$ cross-section. In the meantime, the HF calculation returns quite a smooth and monotonous phase shift. Agreement between the two sets of calculations, the present and the one reported by [31], is very good.

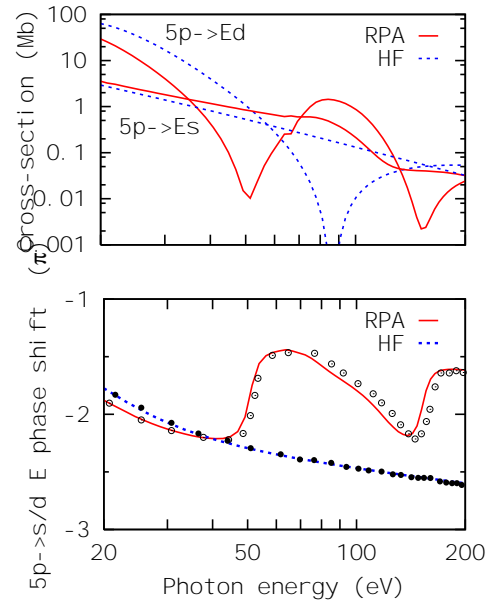


FIG. 6: (Color online) Top: Partial photoionization cross-sections of Xe in the $5p \rightarrow Ed$ and $5p \rightarrow Es$ channels in the RPA (solid red line) and HF (dotted blue line) approximations. Bottom: Phase shift between the partial $5p \rightarrow Ed$ and $5p \rightarrow Es$ waves. The present RPA and HF calculations (solid red and blue dotted lines, respectively) are compared with the RPA and HF calculations reported in Zimmermann et al. [31] (open and filled circles, respectively).

IV. CONCLUSION

In the present work, we perform a systematic study of the photoemission time delay from the valence shells of noble gas atoms in sequence from Ne to Xe. We cover the photon energy range from the ionization threshold to 200 eV. We test the accuracy of our calculation by making comparison with available partial photoionization cross-sections. We derive the complex phase of the photoionization matrix element in the non-relativistic HF and RPA calculations and convert it to the photoelectron group delay by taking the energy derivative.

The time delay results display a very diverse landscape due to an interplay of three major factors. The first two are the logarithmic Coulomb singularity and the Levinson theorem which drive the photoelectron scattering phase in the field of the singly charged ion. The third factor is the phase jump of π near the Cooper's minimum which is smoothed by the inter-shell interaction. The two former factors are revealed in the HF calculations whereas the third one is most vividly reflected in the RPA calculations. Experimentally, photoionization measurements near the Cooper's minima may be challenging but it is the area where the time delay effects are expected to be largest.

These time delay results are compared with experimental data derived from the attosecond streaking mea-

surement [1] and the two-photon interferometric technique [6]. This comparison is inconclusive as the difference between the theoretical and experimental results clearly exceeds the reported error bars. We are fairly confident about the accuracy of the present calculation which is tested by comparison of the partial photoionization cross-sections with a large set of independent experimental data. In the case of Xe, a direct comparison with the scattering phase shift is also performed. Even for this heaviest of the atoms studied in the present work, the relativistic effects are not expected to change considerably the complex phase [6] and hence the associated time delay. It is therefore an open question why the time delay results cannot be verified experimentally. Such a

verification would be a very welcoming development both for the attosecond time delay measuring techniques and the complete theory of atomic photoionization.

Acknowledgement

The author wishes to thank Vladislav Yakovlev and Anne L'Huillier for many useful and stimulating discussions and a critical reading of the manuscript. This work is supported by the Australian Research Council in the form of the Discovery grant DP120101805.

-
- [1] M. Schultze *et al*, *Delay in Photoemission*, Science **328**(5986), 1658 (2010).
- [2] K. Klünder *et al*, *Probing single-photon ionization on the attosecond time scale*, Phys. Rev. Lett. **106**(14), 143002 (2011).
- [3] A. S. Kheifets and I. A. Ivanov, *Delay in atomic photoionization*, Phys. Rev. Lett. **105**(23), 233002 (2010).
- [4] C. A. A. de Carvalho and H. M. Nussenzveig, *Time delay*, Phys. Rep. **364**(2), 83 (2002).
- [5] J. Dahlström, D. Guénot, K. Klünder, M. Gisselbrecht, J. Mauritsson, A. L. Huillier, A. Maquet, and R. Taïeb, *Theory of attosecond delays in laser-assisted photoionization*, Chemical Physics pp. – (2012).
- [6] D. Guénot, K. Klünder, C. L. Arnold, D. Kroon, J. M. Dahlström, M. Miranda, T. Fordell, M. Gisselbrecht, P. Johnsson, J. Mauritsson, *et al.*, *Photoemission-time-delay measurements and calculations close to the 3s-ionization-cross-section minimum in Ar*, Phys. Rev. A **85**, 053424 (2012).
- [7] J. A. R. Samson and J. L. Gardner, *Photoionization cross sections of the outer s-subshell electrons in the rare gases*, Phys. Rev. Lett. **33**, 671 (1974).
- [8] M. Y. Amusia, V. K. Ivanov, N. A. Cherepkov, and L. V. Chernysheva, *Interference effects in photoionization of noble gas atoms outer s-subshells*, Physics Letters A **40**(5), 361 (1972).
- [9] L. R. Moore, M. A. Lysaght, J. S. Parker, H. W. van der Hart, and K. T. Taylor, *Time delay between photoemission from the 2p and 2s subshells of neon*, Phys. Rev. A **84**, 061404 (2011).
- [10] M. Ivanov and O. Smirnova, *How accurate is the attosecond streak camera?*, Phys. Rev. Lett. **107**, 213605 (2011)
- [11] S. Nagele, R. Pazourek, J. Feist, K. Doblhoff-Dier, C. Lemell, K. Tökési, and J. Burgdörfer, *Time-resolved photoemission by attosecond streaking: extraction of time information*, J. Phys. B **44**(8), 081001 (2011).
- [12] S. Nagele, R. Pazourek, J. Feist, and J. Burgdörfer, *Time shifts in photoemission from a fully correlated two-electron model system*, Phys. Rev. A **85**, 033401 (2012).
- [13] M. Y. Amusia, *Atomic photoeffect* (Plenum Press, New York, 1990).
- [14] L. V. Chernysheva, N. A. Cherepkov, and V. Radojevic, *Self-consistent field Hartree-Fock program for atoms*, Comp. Phys. Comm. **11**, 57 (1976).
- [15] L. V. Chernysheva, N. A. Cherepkov, and V. Radojevic, *Frozen core Hartree-Fock program for atomic discrete and continuous states*, Comp. Phys. Comm. **18**, 87 (1979).
- [16] U. Fano, *Propensity rules: An analytical approach*, Phys. Rev. A **32**, 617 (1985).
- [17] M. I. Amusia and L. V. Chernysheva, *Computation of atomic processes : A handbook for the ATOM programs* (Institute of Physics Pub., Bristol, UK, 1997).
- [18] J. Bizau and F. Wuilleumier, *Redetermination of absolute partial photoionization cross sections of he and ne atoms between 20 and 300 ev photon energy*, Journal of Electron Spectroscopy and Related Phenomena **71**(3), 205 (1995), ISSN 0368-2048
- [19] Y. Ralchenko, A. E. Kramida, J. Reader, and NIST ASD Team, *NIST Atomic Spectra Database (version 3.1.5)*, Tech. Rep., National Institute of Standards and Technology, Gaithersburg, MD. (2011).
- [20] M. J. Seaton, *Quantum defect theory*, Rep. Prog. Phys. **46**(2), 167 (1983).
- [21] B. Möbus *et al*, *Measurements of absolute Ar 3s photoionization cross sections*, Phys. Rev. A **47**(5), 3888 (1993).
- [22] J. Samson and W. Stolte, *Precision measurements of the total photoionization cross-sections of He, Ne, Ar, Kr, and Xe*, J. Electr. Spectr. Relat. Phenom. **123**(2-3), 265 (2002), ISSN 0368-2048.
- [23] U. Fano and J. W. Cooper, *Spectral distribution of atomic oscillator strengths*, Rev. Mod. Phys. **40**, 441 (1968).
- [24] A. Ehresmann, F. Vollweiler, H. Schmoranzler, V. L. Sukhorukov, B. M. Lagutin, I. D. Petrov, G. Mentzel, and K. H. Schartner, *Photoionization of Kr 4s. III. Detailed and extended measurements of the Kr 4s-electron ionization cross section*, J. Phys. B **27**(8), 1489 (1994).
- [25] S. Aksela, H. Aksela, M. Levasalmi, K. H. Tan, and G. M. Bancroft, *Partial photoionization cross sections of Kr 3d, 4s, and 4p levels in the photon energy range 37-160eV*, Phys. Rev. A **36**, 3449 (1987).
- [26] Z. Altun and V. Radojevic, *Relaxation effects on the 3d photoionisation of atomic krypton and the bromine negative ion*, J. Phys. B **25**(18), 3757 (1992).
- [27] V. Schmidt, *Photoionization of atoms using synchrotron radiation*, Rep. Prog. Phys. **55**(9), 1483 (1992).

- [28] U. Becker, D. Szostak, H. G. Kerkhoff, M. Kupsch, B. Langer, R. Wehlitz, A. Yagishita, and T. Hayaishi, *Subshell photoionization of Xe between 40 and 1000 eV*, Phys. Rev. A **39**, 3902 (1989).
- [29] A. Fahlman, M. O. Krause, T. A. Carlson, and A. Svensson, *Xe 5s, 5p correlation satellites in the region of strong interchannel interactions, 28-75 eV*, Phys. Rev. A **30**, 812 (1984).
- [30] M. Kutzner, V. Radojević, and H. P. Kelly, *Extended photoionization calculations for xenon*, Phys. Rev. A **40**, 5052 (1989).
- [31] B. Zimmermann, G. Snell, B. Schmidtke, J. Viefhaus, N. A. Cherepkov, B. Langer, M. Drescher, N. Müller, U. Heinzmann, and U. Becker, *Interchannel interaction versus relativistic effects: Xe 5p photoionization revisited*, Phys. Rev. A **64**, 062501 (2001).